

Single layer MoS₂ nanoribbon field effect transistor

D. Kotekar-Patil,^{1,*} J. Deng,¹ S. L. Wong,^{1,2} Chit Siong Lau,¹ and Kuan Eng Johnson Goh^{1,2,†}

¹*Institute of Materials Research and Engineering, Agency for Science Technology and Research,
2 Fusionopolis Way, 08-03 Innovis, 138634, Singapore*

²*Department of Physics, National University of Singapore, 2 Science Drive 3, 117551, Singapore*

We study field effect transistor characteristics in etched single layer MoS₂ nanoribbon devices of width 50 nm with ohmic contacts. We employ a SF₆ dry plasma process to etch MoS₂ nanoribbons using low etching (RF) power allowing very good control over etching rate. Transconductance measurements reveal a steep sub-threshold slope of 3.5V/dec using a global backgate. Moreover, we measure a high current density of 38 $\mu\text{A}/\mu\text{m}$ resulting in high on/off ratio of the order of 10⁵. We observe mobility reaching as high as 50 cm²/V.s with increasing source-drain bias.

2D layered materials such as graphene and transition metal dichalcogenides (TMDs) provide an alternative path towards future nanoscale devices for electronic applications due to their interesting electronic properties. Graphene has been reported to exhibit very high charge mobility¹, but the lack of bandgap in graphene makes it unattractive for transistor applications². Bulk TMDs like MoS₂, WS₂, WSe₂ etc. are semiconducting with indirect bandgap whereas monolayer has a direct and sufficiently large bandgap (1-2eV)³⁻⁸ to allow on and off transistor operations. Among TMD materials, MoS₂ is one of the well explored and broadly studied materials. Additionally, MoS₂ has been reported to exhibit high mobility^{9,10}, high on/off ratio¹¹ along with low contact resistance¹²⁻¹⁴ and ultrashort channel¹⁵ making it an attractive platform for transistor based applications. The ultrathin body of single layer MoS₂ is advantageous for scaling the channel length below 5 nm¹⁶.

In order to implement large scale TMD-based devices using top-down engineering, there are two initial challenges to be overcome:

1. Controlled growth of wafer scale TMDs, with specified number of layer(s) and homogeneity.
2. Controlled etching of TMDs in order to define the active device region, e.g. nanoribbons (NR) which defines a conduction channel.

While advancements in large scale TMD growth is evidenced by the increasing body of works reported¹⁷, relatively less focussed on achieving controlled TMD etching down to the few nm scale with reproducible specifications. Etching can introduce edge roughness and defects which can deteriorate the charge transport in the NR by scattering charge carriers. This is exacerbated in single layer MoS₂ due to the lack of screening in its ultrathin body.

In this manuscript, we investigate field effect transistor (FET) characteristics of 50 nm wide etched NRs. NRs are etched out using a dry SF₆ plasma. Robust ohmic contacts are formed by maximizing the monolayer MoS₂ and metal contact overlap. FET characterization is done by utilizing the global back gate. The associated transfer characteristics reveal high field effect mobility of 50 cm²/V.s, current on/off ratio of 10⁵ and current density (J) 38 $\mu\text{A}/\mu\text{m}$ demonstrating the highest values

reported for TMD NR-FET reported to date for etched single layer MoS₂.

In order to fabricate a NR-FET, a MoS₂ flake was mechanically exfoliated from bulk crystal (2D semiconductors) and transferred on heavily p-doped Si substrate with a 300 nm thick SiO₂ layer on top. The substrate was also used as a back gate to investigate FET characteristics. The substrate with MoS₂ flake was then spin-coated with PMMA A5 and e-beam lithography was performed to define source and drain contacts (fig.1a). Ti/Au (10/80 nm) was evaporated followed by a lift-off step to form ohmic contacts with the MoS₂ (fig.1b). The sample was then annealed at 200 degrees celsius in H₂/Ar atmosphere to ensure good ohmic contact and removal of any remaining resist residue^{11,18}. In order to etch out a NR, the flake was spin-coated again with PMMA A5 (1:1)(fig.1c). This time a thinner PMMA was used to get better e-beam lithographic resolution. E-beam lithography was performed to write a structure such that in the region where NR was desired, PMMA remained unexposed to the e-beam. This PMMA served as a mask to protect MoS₂ underneath it during etching process while the surrounding MoS₂ was etched (fig.1d). After the etching process, the PMMA was removed with acetone leaving a MoS₂-NR between the metallic source-drain contacts (fig.1e).

Multilayer flakes were used to determine the optimal MoS₂ etching rates. An SF₆ dry plasma was used to etch MoS₂ (SF₆: 30 sccm, Pressure: 30 mT, RF source power: 15 W). In order to achieve slower etching rate, we used a reduced RF source power as compared to previous studies^{19,20}. This gave better control over the etching rate and possibly minimizes the edge roughness. With these etching parameters, we estimate an etching rate of 0.2 layer/sec. For monolayer MoS₂-NR devices we always over-etched to ensure complete removal of MoS₂ in the desired area. Fig.1f and 1g shows a series of optimised etched NRs in multi-layer MoS₂ with widths ranging from 50 nm to 185 nm.

Before fabricating the device, optical characterisation was performed to identify monolayer MoS₂ by photoluminescences and Raman spectroscopy. Figs. 2a and 2b show the room temperature photoluminescence measurements (PL) and Raman spectroscopy performed on a

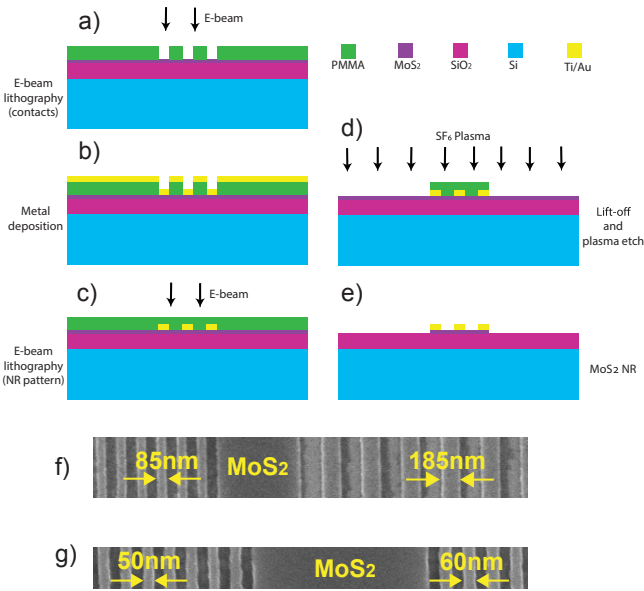


Figure 1. Panels in figs. a-e shows a step-by-step process flow used to etch out a NR from MoS₂ flake. Two e-beam lithography steps are done to fabricate a NR-FET, first to define source and drain contacts and second to define NR structure in PMMA. SF₆ plasma was used to etch out MoS₂ NRs using PMMA as a etch mask. Color code used in schematic for each material in the fabrication process is shown in the legend. Figs. f-g show etched NRs in multilayer MoS₂ flake with different NR width. Fig. f shows 85 and 185 nm NRs whereas fig.g shows 50 nm and 60 nm NRs.

flake shown in the inset of fig.2a. Both the optical characterisations were performed using a 532 nm laser. A PL peak centred at 670 nm in fig. 2a indicates the presence of direct bandgap, a hallmark of monolayer MoS₂. This peak at 670 nm corresponds to 1.85eV, a value consistent with the reported bandgap of monolayer MoS₂^{21,22}. For multilayer MoS₂ flakes, PL traces (not shown) exhibit multiple emission peaks with weak PL intensities that further reassures that our sample is a monolayer MoS₂ flake. Raman spectroscopy performed using the same laser wavelength (532 nm) shows the characteristic out-of-plane Raman mode (A_{1g}) and the in-plane mode (E_{2g}) separated by $\Delta\gamma=19\text{ cm}^{-1}$, which agrees well with other reports of monolayer MoS₂^{21,23,24}. Devices D1 and D2 were fabricated on a monolayer flake shown in inset of fig. 2a while D3 on another monolayer flake (identified by optical contrast).

All the electrical measurements shown in this work were performed on a Janis probe station at room temperature and under vacuum ($<10^{-4}$ mTorr). Two-terminal source-drain current (I_d) was measured by applying a source-drain bias voltage (V) across the device and the channel carrier density modulated by the backgate (V_{bg}). Figs. 2c and 2d shows the logarithmic source-drain current (I_d) traces as a function of V_{bg} for three monolayer MoS₂ NR-FET devices (D1-D3) at $V=0.1$ V and

$V=1$ V respectively. All three devices have a channel of width (W)=50 nm and channel length (L)=500 nm. Typical threshold voltage (V_{th}) measured in MoS₂ FETs with global back gate are negative values²⁵. We also found negative FET threshold voltages (-30 to -10 V) in all our MoS₂ devices after step b) in Fig.1, before the NR etching step. This is in agreement with the threshold voltages in our MoS₂ FETs [-30 to -10 V] before etching it into NRs. After etching the flakes into NRs of width (W)=50 nm, we see a shift towards positive threshold voltage indicating a transition from depletion mode to accumulation mode in NR FET consistent with previous studies²⁶. For all the three NR-FET devices (D1-D3), we find a positive threshold voltage in the range 20-35 V at $V=0.1$ V which is extracted using the field effect mobility fit in the linear part of the I_d region (see below for further discussion). From fig. 2c and 2d, we note that device D1 has slightly higher I_d and steeper sub-threshold slope (SS) compared to other two devices (D2 and D3). For the rest of the text in this manuscript we focus on the FET characteristics of D1 and for other devices the results are summarize in the table I.

A device exhibiting steep SS allows faster switching between the on- (high current) and the off- (low current) states of FETs. At $V=1$ V, D1 has a $SS=3.5$ V/dec. This value of SS is almost three times steeper than the previous NR-FET value reported of comparable dimensions²⁶. We achieve steeper SS since our devices are fabricated from single layer MoS₂ which provide better electrostatic control over the channel as compared to multilayer channel. From the SS value, one can extract the interface charge traps using $SS = \frac{2.3k_B T}{q} (1 + \frac{C_{it}}{C_{ox}})$, where k_B : Boltzmann constant, T=temperature, q=electron charge, C_{it} =interface trap capacitance, C_{ox} = gate oxide capacitance^{25,26}. Using $C_{ox}(= \frac{\epsilon_0 \epsilon_r}{d})=1.15 \times 10^{-4}$ F/m² gives interface trap density of $D_{it}=2.29 \times 10^{12}/\text{cm}^2\text{-eV}$. The extracted trap density in our single layer MoS₂ FET is better than typical value reported for NR-FET in multilayer devices²⁶. In order to estimate the SS in a top gated device, we consider a 5 nm thick hafnium oxide (dielectric constant=25) and assume a same interface trap density to get $SS \approx 69$ mV/dec. This estimated SS is consistent with the measured SS in single layer MoS₂ FET using hafnium oxide as gate dielectric¹¹.

Fig. 3a shows the output characteristics of the device D1. Each I_d vs V trace was taken at a fixed V_{bg} ranging from -20 to 60 V. The output characteristic curves are linear at low V exhibiting ohmic behavior, indicating a narrow Schottky barrier. The curves tend to saturate at higher V due to carrier velocity saturation. The saturation I_d gives the on-state current of the FET. The saturation I_d at $V=2$ V and $V_{bg}=60$ V is $38 \mu\text{A}/\mu\text{m}$ giving a on/off ratio of $\approx 10^5$. The high current density of $38 \mu\text{A}/\mu\text{m}$ in our single layer NR-FET is comparable to the current density in 6 nm thick NR-FET²⁰. This suggests that our etching process did not degrade the device performance significantly. The on/off ratio should be considered as the lower limit since we are limited by

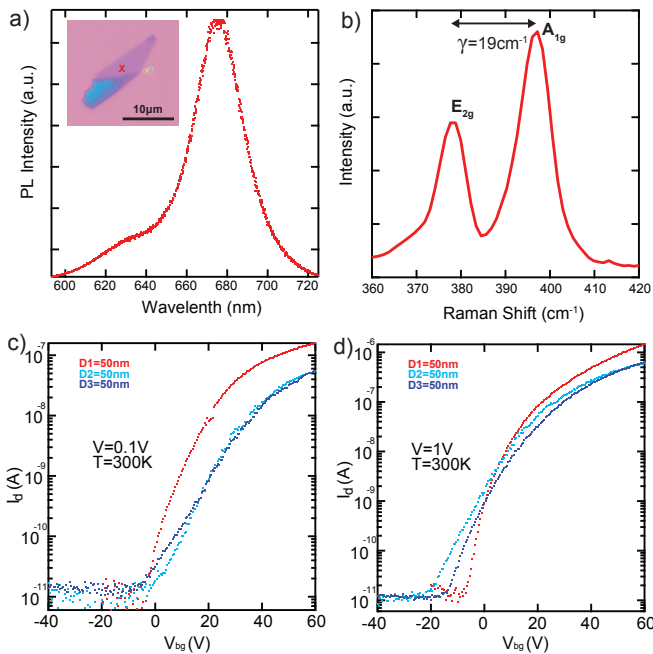


Figure 2. a) Room temperature PL measurement showing a strong PL peak at 670 nm associated with direct bandgap in monolayer MoS₂. b) Room temperature Raman spectroscopy showing two peaks at 378.12 cm⁻¹ and 397.18 cm⁻¹ separated by $\Delta\gamma = 19$ cm⁻¹ associated with characteristic E_{2g} and A_{1g} peaks of single layer MoS₂ respectively. c) and d) showing logarithmic I_d vs V_{bg} at $V = 0.1$ V and $V = 1$ V respectively.

the off-state current (≈ 10 pA) which is 2 orders of magnitude higher than previous report on multilayer NR-FET of similar dimensions^{26,27}. From the linear region of the output characteristic, field effect mobility can be extracted using the equation $\mu = \frac{L}{WC_{ox}V} \frac{dI_d}{dV_{bg}}$ without subtracting the contact resistance^{25,26,28}. Fig. 3b shows the I_d vs V_{bg} at $V = 0.6$ V. Black line overlapping the linear part of I_d in fig.3b is the mobility fit using $W = 50$ nm and $L = 500$ nm which gives a mobility of 50 cm²/V.s. Fig.3c shows the field effect mobility as a function of V . We observe that the mobility increases with increase in V and reaches a value of $\mu = 50$ cm²/V.s at $V = 0.6$ V. This increase in mobility with V indicates thinning of Schottky barrier width at higher V resulting in efficient injection of charge carriers. Comparing the device properties of D1 with the other two devices, D2 and D3 in table 1, we observe variability in transport characteristics. Even

though all the devices are fabricated at the same time with identical process, device characteristics may have variations from device to device depending on the microscopic details of the single layer MoS₂, its interface with the substrate, and also the uncertainties introduced by the fabrication process..

To conclude, we have demonstrated a NR-FET etched in a monolayer MoS₂ of width 50 nm with steep sub-threshold slope. Moreover, we observe increasing mobility with source-drain voltage reaching up to $\mu =$

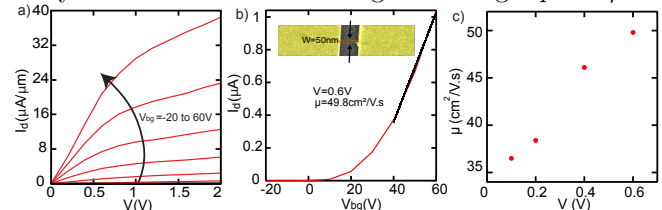


Figure 3. a) Transfer output characteristic of 50 nm NR-FET device (D1). Each trace is measured at different back gate voltage varying from $V_{bg} = -20$ to 60 V. I_d traces increase linearly at low V and approach saturation at high V . b) Linear I_d vs V_{bg} at $V = 0.6$ V. Black line overlapping the I_d trace is a linear fit to extract mobility. Inset shows false color SEM image of the NR device on which measurement is performed. c) Mobility plotted as a function of V .

50 cm²/V.s. Further improvement in mobility can be achieved by using a mobility boosting high- k dielectric like HfO₂. From the transfer characteristic, we find a significant on/off ratio of at least 10⁵ could be attained even with a back-gated configuration.. This work demonstrates a significant milestone in the development of etching monolayer TMDs down to the nm regime, showing that high mobilities in the range of few tens of cm²/V.s is attainable in the first devices fabricated thus.

ACKNOWLEDGMENTS

This work was supported by the A*STAR (Singapore) QTE Grant No. A1685b0005.

REFERENCES

* patild@imre.a-star.edu.sg

† kejpgoh@yahoo.com

¹ J. H. Chen, C. Jang, S. Xiao, M. Ishigami, and M. S. Fuhrer, ArXiv e-prints (2007), arXiv:0711.3646 [cond-mat.mtrl-sci].

² K. S. Novoselov, A. K. Geim, S. V. Morozov, D. Jiang, M. I. Katsnelson, I. V. Grigorieva, S. V. Dubonos, and

A. A. Firsov, Nature (London) **438**, 197 (2005), cond-mat/0509330.

³ K. F. Mak, C. Lee, J. Hone, J. Shan, and T. F. Heinz, Physical Review Letters **105**, 136805 (2010), arXiv:1004.0546 [cond-mat.mtrl-sci].

⁴ S. Tongay, W. Fan, J. Kang, J. Park, U. Koldemir, J. Suh, D. S. Narang, K. Liu, J. Ji, J. Li, R. Sinclair, and

Table I. Table summarizing the NR-FET parameters

Device#	L(nm)	W(nm)	V_{th} (V)	μ ($\text{cm}^2/\text{V}\cdot\text{s}$)	D_{it} ($10^{12}/\text{cm}^2\text{-eV}$)	SS(V/dec)	on/off ratio	J ($\mu\text{A}/\mu\text{m}$)
D1	500	50	20	50	2.29	3.5	1.9×10^5	38
D2	500	50	31	15.1	13.8	11.5	1.2×10^5	24
D3	500	50	33.4	31	7.8	6.5	1×10^5	20

- J. Wu, *Nano Letters* **14**, 3185 (2014), pMID: 24845201, <https://doi.org/10.1021/nl500515q>.
- ⁵ X. Lu, M. I. B. Utama, J. Lin, X. Gong, J. Zhang, Y. Zhao, S. T. Pantelides, J. Wang, Z. Dong, Z. Liu, W. Zhou, and Q. Xiong, *Nano Letters* **14**, 2419 (2014), pMID: 24678857, <https://doi.org/10.1021/nl5000906>.
- ⁶ W. Zhao, Z. Ghorannevis, L. Chu, M. Toh, C. Kloc, P.-H. Tan, and G. Eda, *ACS Nano* **7**, 791 (2013), pMID: 23256505, <https://doi.org/10.1021/nn305275h>.
- ⁷ Y. Zhang, T.-R. Chang, B. Zhou, Y.-T. Cui, H. Yan, Z. Liu, F. Schmitt, J. Lee, R. Moore, Y. Chen, H. Lin, H.-T. Jeng, S.-K. Mo, Z. Hussain, A. Bansil, and Z.-X. Shen, *Nature Nanotechnology* **9**, 111 (2014), arXiv:1401.3386 [cond-mat.mtrl-sci].
- ⁸ B. W. H. Baugher, H. O. H. Churchill, Y. Yang, and P. Jarillo-Herrero, *Nature Nanotechnology* **9**, 262 (2014).
- ⁹ Y. Liu, J. Guo, E. Zhu, L. Liao, S.-J. Lee, M. Ding, I. Shakir, V. Gambin, Y. Huang, and X. Duan, *Nature* **557**, 696 (2018).
- ¹⁰ R. Pisoni, Z. Lei, P. Back, M. Eich, H. Overweg, Y. Lee, K. Watanabe, T. Taniguchi, T. Ihn, and K. Ensslin, *Applied Physics Letters* **112**, 123101 (2018), arXiv:1801.00452 [cond-mat.mes-hall].
- ¹¹ B. Radisavljevic, A. Radenovic, J. Brivio, V. Giacometti, and A. Kis, *Nature Nanotechnology* **6**, 147 (2011).
- ¹² W. Liu, J. Kang, W. Cao, D. Sarkar, Y. Khatami, D. Jena, and K. Banerjee, in *2013 IEEE International Electron Devices Meeting* (2013) pp. 19.4.1–19.4.4.
- ¹³ L. Yang, K. Majumdar, H. Liu, Y. Du, H. Wu, M. Hatzistergos, P. Y. Hung, R. Tieckelmann, W. Tsai, C. Hobbs, and P. D. Ye, *Nano Letters* **14**, 6275 (2014), pMID: 25310177, <https://doi.org/10.1021/nl502603d>.
- ¹⁴ Y. Liu, J. Guo, Y. Wu, E. Zhu, N. O. Weiss, Q. He, H. Wu, H.-C. Cheng, Y. Xu, I. Shakir, Y. Huang, and X. Duan, *Nano Letters* **16**, 6337 (2016).
- ¹⁵ S. B. Desai, S. R. Madhvapathy, A. B. Sachid, J. P. Llinas, Q. Wang, G. H. Ahn, G. Pitner, M. J. Kim, J. Bokor, C. Hu, H.-S. P. Wong, and A. Javey, *Science* **354**, 99 (2016), <http://science.sciencemag.org/content/354/6308/99.full.pdf>.
- ¹⁶ D. S. Schulman, A. J. Arnold, and S. Das, *Chem. Soc. Rev.* **47**, 3037 (2018).
- ¹⁷ S. Manzeli, D. Ovchinnikov, D. Pasquier, O. V. Yazyev, and A. Kis, *Nature Reviews Materials* **2**, 17033 (2017).
- ¹⁸ M. Ishigami, J. H. Chen, W. G. Cullen, M. S. Fuhrer, and E. D. Williams, *Nano Letters* **7**, 1643 (2007), pMID: 17497819, <https://doi.org/10.1021/nl070613a>.
- ¹⁹ S. Xiao, P. Xiao, X. Zhang, D. Yan, X. Gu, F. Qin, Z. Ni, Z. J. Han, and K. K. Ostrikov, *Scientific Reports* **6**, 19945 (2016).
- ²⁰ F. Zhang, C.-H. Lee, J. A. Robinson, and J. Appenzeller, *Nano Research* **11**, 1768 (2018).
- ²¹ Y.-F. Lim, K. Priyadarshi, F. Bussolotti, P. K. Gogoi, X. Cui, M. Yang, J. Pan, S. W. Tong, S. Wang, S. J. Pennycook, K. E. J. Goh, A. T. S. Wee, S. L. Wong, and D. Chi, *ACS Nano* **12**, 1339 (2018), pMID: 29338197, <https://doi.org/10.1021/acsnano.7b07682>.
- ²² A. Splendiani, L. Sun, Y. Zhang, T. Li, J. Kim, C.-Y. Chim, G. Galli, and F. Wang, *Nano Letters* **10**, 1271 (2010), pMID: 20229981, <https://doi.org/10.1021/nl903868w>.
- ²³ Y.-H. Lee, X.-Q. Zhang, W. Zhang, M.-T. Chang, C.-T. Lin, K.-D. Chang, Y.-C. Yu, J. Tse-Wei Wang, C.-S. Chang, L.-J. Li, and T.-W. Lin, *ArXiv e-prints* (2012), arXiv:1202.5458 [cond-mat.mtrl-sci].
- ²⁴ S. Wu, C. Huang, G. Aivazian, J. S. Ross, D. H. Cobden, and X. Xu, *ACS Nano* **7**, 2768 (2013), pMID: 23427810, <https://doi.org/10.1021/nn4002038>.
- ²⁵ W. Liu, D. Sarkar, J. Kang, W. Cao, and K. Banerjee, *ACS Nano* **9**, 7904 (2015), pMID: 26039221, <https://doi.org/10.1021/nn506512j>.
- ²⁶ H. Liu, J. Gu, and P. D. Ye, *IEEE Electron Device Letters* **33**, 1273 (2012).
- ²⁷ S. Fathipour, M. Remskar, A. Varlec, A. Ajoy, R. Yan, S. Vishwanath, S. Rouvimov, W. S. Hwang, H. G. Xing, D. Jena, and A. Seabaugh, *Applied Physics Letters* **106**, 022114 (2015), arXiv:1411.6000 [cond-mat.mes-hall].
- ²⁸ D. Kotekar-Patil, B.-M. Nguyen, J. Yoo, S. A. Dayeh, and S. M. Frolov, *Nanotechnology* **28**, 385204 (2017), arXiv:1611.02722 [cond-mat.mes-hall].